JOURNAL OF THEORETICAL
AND APPLIED MECHANICS
https://doi.org/10.15632/jtam-pl/200383
ONLINE FIRST

BIFURCATION CHARACTERISTICS AND CONTROL OF FRICTION SELF-EXCITED VIBRATION SYSTEM OF COKE PUSHING

Junjun CHEN*, Bing XU, Ge YAN

School of Automation and Software Engineering, Shanxi University, Taiyuan 030031, China
*corresponding author, *chenjunjun7505179@163.com*

There are typical friction self-excited vibration phenomena such as stick-slip and flutter in the working process of a coke pushing device. For the purpose of studying the vibration mechanism, a mechanical model of friction self-excited vibration of a double-mass-conveyor belt is established based on the Stribeck friction effect. Mass 1 and mass 2 are used to represent the part entering the carbonization room and the part outside the carbonization room, and the stability and bifurcation characteristics of the two masses are studied. The results show that the critical instability velocity and bifurcation velocity of the two masses are the same. Then the linear and nonlinear state feedback controller is designed to control the velocity bifurcation points and limit cycles of the coke pushing system. The numerical simulation results show that the appropriate selection of linear gain can reduce the bifurcation velocity and ensure the stability of the system at low velocity, and the appropriate selection of nonlinear gain can reduce the amplitude of the limit cycle and reduce the intensity of self-excited vibration of the coke pushing device.

Keywords: self-excited vibration; friction model; coke pushing system; bifurcation; linear and nonlinear state feedback.

1. Introduction

The mechanical device studied in this paper is a kind of coke pushing device, its function is to push coke out of the carbonization chamber (Chen *et al.*, 2019; 2020). In the process of pushing red coke out of the carbonization chamber, the coke pushing rod entering the carbonization chamber contacts the ground through the sliding shoe to form sliding friction. In the process of pushing coke, there is strong and complicated friction between the sliding shoe and the carbonizing chamber floor. Through the monitoring of the production process, we can see that there is an obvious flutter phenomenon when pushing the coke. Moreover, the vibration exhibits typical friction-induced vibration. Usually, the unwanted vibrations will cause wear of the contacting parts, surface damage, fatigue damage and noise, and it also will have a great impact on working performance, operation reliability, and service life of the coke pushing device.

We often find friction-induced vibrations in mechanical systems and in daily life, such as squeaky windshield wipers, the sound of certain arcuate instruments, the flutter of machine tools, the brake noise of automobile and stick-slip vibration of drill pipe (Kinkaid *et al.*, 2003). In the field of engineering, many scholars and engineers have conducted in-depth research on automobile braking noise. Of course, many published papers have also investigated various dynamic behaviours of friction-excited systems. Popp *et al.* (1995) investigated discrete and continuous models including stick-slip motion and bifurcation and demonstrated chaotic phenomena. Elmaian *et al.* (2014) described three modes of motion, stick, slip and separation in a three-degree-of-freedom (3-DOF) model incorporating friction-induced vibration. Zhang *et al.* (2018) introduced a flexible pin-on-disc system to reveal the process of generating noise in friction con-

tact, and researched the periodic friction coefficient effect on the features of time-varying squeal. Kruse *et al.* (2015) studied the influence of joints on the dynamic characteristics of a friction-induced flutter system. Brunetti *et al.* (2016) established a periodic modular lumped model to study its dynamic properties. Pilipchuk *et al.* (2015) studied the non-stationary mechanism of a 2-DOF braking model in the vibration caused by friction. The results show that the responses of the system change qualitatively as the velocity of the belt decreases. Wei *et al.* (2019) simulated a brake system with a 3-DOF mechanical model, and indicated bifurcation and chaotic phenomena. Denimal *et al.* (2020) proposed a new method to determine the degree of influence of unstable modes in a nonlinear self-excited vibration response, and which is also used to estimate the limit cycle. Lima and Sampaio (2020) analyzed a multi-physical system with stick-slip oscillation in the interaction of mechanical subsystem and electromagnetic subsystem. Papangelo *et al.* (2018) found that there were several local vibration states in the weakly coupled friction-excited oscillator chain. Von Wagner *et al.* (2007) analyzed the stability characteristics of the oscillating disc brake model. Sui and Ding (2018) studied the instability of the pad in the motion interaction of the disc and carried out the random analysis. Li *et al.* (2018) and Wang *et al.* (2020) verified experimentally the low degree of freedom models simulated numerically, and the friction-induced vibration of the system on the real test bench. Liu and Ouyang (2020) investigated the friction-induced vibration of a new model consisting of 5-DOF mass oscillating band including various nonlinearities. Without doubt, 1-DOF mechanical models containing mass blocks and constant velocity belts have been widely used to study vibration mechanism caused by friction (Wang *et al.*, 2022). A great deal of research has also been done on the sources of nonlinearity in friction-induced vibration problems, such as the nonlinearity of the contact stiffness, non-smooth characteristics such as stick-slip and contact/separation. However, there is a lack of comprehensive analysis of the effects of various nonlinearities on friction-induced self-excited vibration.

After in-depth research, three main mechanisms by which friction drives oscillations have been proposed. One of the main mechanisms is the Stribeck effect which is characterized by velocity weakening characteristics. In contrast, two other widely investigated mechanisms are called model-coupling and sprag-slip instability. We already know that friction-induced vibration is unacceptable in many systems. And rich dynamic behaviours often appear in friction-induced vibration. Saha *et al.* (2016) experimentally studied a test device representing a friction-induced system with 1-DOF and showed the properties of bifurcations related to friction instability of the system. Veraszto and Stepan (2017) investigated stability and bifurcation behaviours in digital and Saha *et al.* (2016) mentioned a continuous systems on the basis of 1-DOF nonlinear mechanical model. It is also necessary to effectively control the dynamic behaviours caused by friction vibration. In recent years, there have been many papers on how to control the friction-induced vibration. Nonlinear state feedback control is one of the control methods, which can realize the precise control of the system by feeding the state of the system back to the controller. When controlling a frictional self-excited vibration system, the output of the nonlinear state feedback controller is a nonlinear function of the system state, which can be designed according to the characteristics and control objectives of the system. By selecting suitable nonlinear functions, the system can maintain good control performance under various working conditions, and has strong robustness to the change of system parameters and external interference. Different active and passive vibration control methods were proposed in literature. Adaptive control is a widely used method in the control system, which can realize the stability control of the system when the system parameters are unstable or uncertain. The basic principle of adaptive control is to realize the stability control of the system by estimating the uncertain parameters online and adjusting the control coefficient in time. This involves establishing the mathematical model of the system, using the parameter estimation and control algorithm to realize real-time adjustment of the dynamic characteristics of the system. Of course, the technical challenges of adaptive control include model stability and robustness, real-time performance, and accuracy of param-

eter estimation. Robust control is also a frequently used control method that aims to design a control system that can maintain stability and performance in the face of model uncertainties, external perturbations, and parameter changes. H_∞ control theory is one of the most commonly used methods in robust control. The controller is designed by optimizing the H_∞ norm of the control system, which represents the maximum gain of the system from input to output and is used to measure the system's ability to suppress disturbances. Robust control is an important branch of the modern control theory, which is very important to solve the uncertainty problem in complex systems. By understanding and applying the robust control theory, the performance and reliability of the system in the face of uncertainty can be improved. The linear and nonlinear state feedback is a combination of linear and nonlinear state feedback control. The theory of linear state feedback control is mature, easy to implement, and very effective for linear systems and linear parts of nonlinear systems. Nonlinear state feedback control is suitable for nonlinear systems and can provide better control performance and robustness.

However, few scholars have studied the bifurcation characteristics of the pushing coke and how to control the vibration of this device. Therefore in this paper, a 2-DOF mass-on-conveyor belt model including friction-induced vibration is proposed, and the bifurcation characteristics and control methods of pushing coke are studied. The dual-mass conveyor system is also very widely used in practical applications, such as the security conveyor of airport railway stations, the conveyor belt of beverage production companies to transmit beverage bottles, and the carton production transmission belt. In the field of industry and agriculture, there is also the improvement of the dual-mass conveyor model to transport the whole bag of cement, the whole bag of rice, the whole packing box, and other items from a low place to a certain height according to the inclination angle. Without doubt, studying the friction-induced vibration of pushing coke has good theoretical and engineering value for manufacturers.

The organizational structure of the paper is arranged as follows. In Section 2, a dynamic model of friction self-excited vibration of a double-mass-conveyor belt is established according to the working characteristics of pushing coke. In Section 3, the stability and bifurcation characteristics of the coke pushing system are analyzed by the theoretical calculation and numerical simulation. Then the linear and nonlinear state feedback controller is put forward to control the bifurcation behavior of the system in Section 4. The linear gain is used to control the change of the bifurcation velocity point, and the nonlinear gain is used to control the size of the limit cycle of the coke pushing system. The research conclusions of this paper are drawn in Section 5.

2. Establishment of mechanical model of coke pushing system

The device of pushing coke is a specific actuator to push the red coke out of the carbonization chamber. Its main structure includes a coke pushing ram, a rack and pinion transmission mechanism, a sliding shoe, a coke pushing head and several supporting rollers. The specific structure of the device of pushing coke is shown in Fig. 1. The device is a large mechanical equipment, in which the length of the pushing ram is nearly 30 meters and the weight is about 40 tons. Due to high temperature and closed coke pushing environment, it is very difficult to carry out experimental researches on such a large equipment.

The establishment of the mechanical model of the system can well reveal the dynamic characteristics of the coke pushing device in theory, which is helpful to further study the self-excited vibration of the device and provide theoretical support for engineering application. In order to study the complex dynamic phenomena during the operation of the coke pushing device, considering the fact that the ram of pushing coke is partly in the carbonization chamber and partly in the carbonization outdoor during the operation of pushing coke, based on the Stribeck friction effect (Thomsen & Fidlin, 2003), the double mass-conveyor belt friction self-excited vibration model is established in Fig. 2.

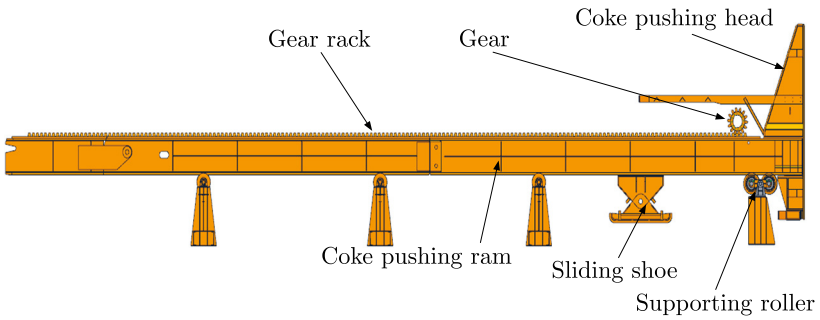

Fig. 1. Main structure of coke pushing device.

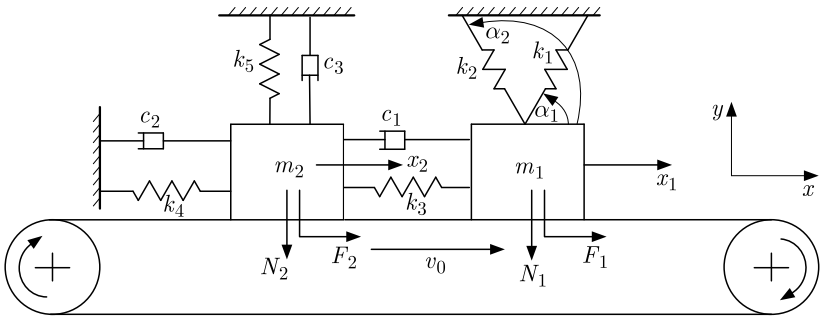

Fig. 2. Mechanical model of coke pushing friction self-excited vibration system.

The conveyor belt moves continuously and unidirectionally with velocity v_0, the part of the coke pushing ram entering the carbonization chamber is represented by mass m_1, while the part of the coke pushing ram outside the carbonization chamber is represented by mass m_2. The positive pressures of m_1 and m_2 applied on the conveyor belt are N_1 and N_2, respectively. The friction forces generated by positive pressures are F_1 and F_2, respectively. The displacement of m_1 and m_2 driven by friction is x_1 and x_2, respectively, and where k_i $(i = 1, ..., 5)$ is the stiffness coefficient, c_1 and c_2 represent the damping coefficients of the system. The differential equation of coke pushing system is

$$\begin{aligned} F_1 &= m_1\ddot{x}_1 + c_1(\dot{x}_1 - \dot{x}_2) + k_3(x_1 - x_2) + k_2 x_1 \cos^2\alpha_2 - k_1 x_2 \cos^2\alpha_1, \\ F_2 &= m_2\ddot{x}_2 + c_2\dot{x}_2 + k_4 x_2 - c_1(\dot{x}_1 - \dot{x}_2) - k_3(x_1 - x_2). \end{aligned} \tag{2.1}$$

In Eq. (2.1), friction F_1 and F_2 are calculated using the Stribeck friction model (Thomsen & Fidlin, 2003), and the expression is

$$\begin{aligned} F_i &= \mu(v_r)N_i, \\ \mu(v_r) &= -\mu_s \operatorname{sgn}(v_r) + \frac{3(\mu_s - \mu_m)}{2v_m} v_r - \frac{(\mu_s - \mu_m)}{2v_m^3} v_r^3, \\ v_r &= \dot{x}_i - v_0, \qquad i = 1, 2, \end{aligned} \tag{2.2}$$

where v_r is the relative sliding velocity between the mass and the conveyor belt, μ_s is the coefficient of static friction, μ_m is the coefficient of dynamic friction, v_m represents the running velocity of the system corresponding to the minimum coefficient of dynamic friction, N_i is the positive pressure originates in the mass and the conveyor belt, and μ represents the friction coefficient of the Stribeck model.

Let $\omega = \sqrt{k_4/m_2}$, $L = N_2/k_3$, the following dimensionless variables are obtained:

$$\begin{aligned}
&\tau = \omega t, && X_1 = x_1 k_3/N_2, && X_2 = x_2 k_3/N_2,\\
&\xi_1 = m_1\omega^2/k_3, && \xi_2 = m_2\omega^2/k_3, && a_1 = c_1\omega/k_3,\\
&a_2 = c_2\omega/k_3, && \beta = N_1/N_2, && \beta_1 = k_4/k_3,\\
&\beta_2 = k_1\cos^2\alpha_1/k_3, && \beta_3 = k_2\cos^2\alpha_2/k_3, && V_0 = \upsilon_0/\omega L,\\
&\dot{X}_1 = \mathrm{d}X_1/\mathrm{d}\tau, && \dot{X}_2 = \mathrm{d}X_2/\mathrm{d}\tau,
\end{aligned} \tag{2.3}$$

where τ means the dimensionless time, X_1 means the dimensionless displacement of mass m_1, and $\dot{X}_1$ means the dimensionless velocity of mass m_1. X_2 means the dimensionless displacement of mass m_2, and $\dot{X}_2$ means the dimensionless velocity of mass m_2. By introducing the aforementioned dimensionless variables, the dimensionless motion equation of the system is obtained:

$$\begin{aligned}
\beta\mu_1 &= \xi_1\ddot{X}_1 + a_1(\dot{X}_1 - \dot{X}_2) + (1 - \beta_2 + \beta_3)X_1 - X_2,\\
\mu_2 &= \xi_2\ddot{X}_2 + a_2\dot{X}_2 - a_1(\dot{X}_1 - \dot{X}_2) - X_1 + (1 + \beta_1)X_2.
\end{aligned} \tag{2.4}$$

Among which,

$$\mu_i = -\mu_s\,\mathrm{sgn}(\dot{X}_i - V_0) + \frac{3(\mu_s - \mu_m)}{2\upsilon_m}(\dot{X}_i - V_0) - \frac{(\mu_s - \mu_m)}{2\upsilon_m^3}(\dot{X}_i - V_0)^3, \qquad i = 1, 2. \tag{2.5}$$

Based on the simplification method in ordinary differential equations, the normal high-order differential equations can be simplified into equivalent first-order differential equations to analyze and calculate more conveniently. Let: $X_1 = Y_1$, $\dot{X}_1 = Y_2$, $X_2 = Y_3$, $\dot{X}_2 = Y_4$, we can get the first order differential equations:

$$\begin{aligned}
\dot{Y}_1 &= Y_2, \qquad \dot{Y}_2 = \frac{-a_1(Y_2 - Y_4) - (1 - \beta_2 + \beta_3)Y_1 + Y_3 + \beta\mu_1}{\xi_1},\\
\dot{Y}_3 &= Y_4, \qquad \dot{Y}_4 = \frac{-a_2Y_4 + a_1(Y_2 - Y_4) + Y_1 - (1 + \beta_1)Y_3 + \mu_2}{\xi_2}.
\end{aligned} \tag{2.6}$$

3. Analysis of bifurcation behaviors of the coke pushing system

When the velocity of the transmission belt in the system reaches a certain value, the mass will meet the static equilibrium state under the interaction of friction and restoring force. At the moment, the system satisfies $X_1' = 0$, $X_2' = 0$, and the sign function of the friction coefficient of the Stribeck model in Eq. (2.2) is $\mathrm{sgn}(\upsilon_r) = -1$. According to the actual data obtained from the production of the enterprise and the actual test of the coke pushing operation site, the coefficient of static friction, the coefficient of dynamic friction, and the running velocity of the system under condition of the minimum dynamic friction coefficient are, respectively, set as $\mu_s = 0.8$, $\mu_m = 0.6$, $\upsilon_m = 0.45$.

Based on the Lyapunov stability theory, the equilibrium point stability of the coke pushing system is analyzed. When $Y_2 = 0$, $Y_4 = 0$, the equilibrium point of the system can be obtained from Eq. (2.6):

$$\begin{aligned}
Y_{10} &= \frac{-\beta(1 + \beta_1)\mu_1 - \mu_2}{-(1 + \beta_1)(1 - \beta_2 + \beta_3) + 1}, && Y_{20} = 0,\\
Y_{30} &= (1 - \beta_2 + \beta_3)\frac{-\beta(1 + \beta_1)\mu_1 - \mu_2}{-(1 + \beta_1)(1 - \beta_2 + \beta_3) + 1} - \beta\mu_1, && Y_{40} = 0.
\end{aligned} \tag{3.1}$$

By moving the system's equilibrium point to the zero point, the equations can be obtained:

$$Y_1 = \widehat{Y}_1 + Y_{10}, \qquad Y_2 = \widehat{Y}_2, \qquad Y_3 = \widehat{Y}_3 + Y_{30}, \qquad Y_4 = \widehat{Y}_4. \tag{3.2}$$

The disturbance equation of the original system is

$$\begin{aligned} \dot{\widehat{Y}}_1 &= \widehat{Y}_2, \qquad \dot{\widehat{Y}}_2 = \frac{-a_1(Y_2 - Y_4) - (1 - \beta_2 + \beta_3)\widehat{Y}_1 + \widehat{Y}_3 + \beta\mu_1}{\xi_1}, \\ \dot{\widehat{Y}}_3 &= \widehat{Y}_4, \qquad \dot{\widehat{Y}}_4 = \frac{-a_2 Y_4 + a_1(Y_2 - Y_4) + \widehat{Y}_1 - (1 + \beta_1)\widehat{Y}_3 + \mu_2}{\xi_2}. \end{aligned} \tag{3.3}$$

In which,

$$\begin{aligned} \mu_1 &= -\mu_s \operatorname{sgn}(Y_2 - V_0) + \frac{3(\mu_s - \mu_m)}{2\upsilon_m}(Y_2 - V_0) - \frac{(\mu_s - \mu_m)}{2\upsilon_m^3}(Y_2 - V_0)^3, \\ \mu_2 &= -\mu_s \operatorname{sgn}(Y_4 - V_0) + \frac{3(\mu_s - \mu_m)}{2\upsilon_m}(Y_4 - V_0) - \frac{(\mu_s - \mu_m)}{2\upsilon_m^3}(Y_4 - V_0)^3. \end{aligned} \tag{3.4}$$

By the Taylor series expansion on the right side of Eq. (3.3) and omitting the second and above terms, we can get the first-order approximate equations of the coke pushing system. When $\widehat{Y}_1 = 0$, $\widehat{Y}_2 = 0$, $\widehat{Y}_3 = 0$, $\widehat{Y}_4 = 0$, the Jacobian matrix of the first-order differential equations of the coke pushing system relative to the variables $\widehat{Y}_1$, $\widehat{Y}_2$, $\widehat{Y}_3$, $\widehat{Y}_4$ can be obtained from Eq. (3.3) as follows:

$$\mathbf{A} = \begin{bmatrix} 0 & 1 & 0 & 0 \\ a_{21} & a_{22} & \dfrac{1}{\xi_1} & \dfrac{a_1}{\xi_1} \\ 0 & 0 & 0 & 1 \\ \dfrac{1}{\xi_2} & \dfrac{a_1}{\xi_2} & a_{43} & a_{44} \end{bmatrix}. \tag{3.5}$$

In which,

$$\begin{aligned} a_{21} &= \frac{\beta_2 - \beta_3 - 1}{\xi_1}, \qquad a_{22} = \frac{-a_1 + 0.67 - 3.3V_0^2}{\xi_1}, \\ a_{43} &= -\frac{1 + \beta_1}{\xi_2}, \qquad a_{44} = \frac{-a_1 - a_2 + 0.67 - 3.3V_0^2}{\xi_2}. \end{aligned} \tag{3.6}$$

The system's dimensionless parameters are set to: $\xi_1 = \xi_2 = 0.1$, $a_1 = a_2 = 0.01$, $\beta = 1$, $\beta_1 = 1.5$, $\beta_2 = \beta_3 = 0.01$. Substituting the above parameters into Eq. (3.5), the corresponding characteristic equation of matrix $\mathbf{A}$ is

$$\begin{aligned} |\lambda\mathbf{E} - \mathbf{A}| = \lambda^4 &+ (66V_0^2 - 13.1)\lambda^3 + (1089V_0^4 - 432.3V_0^2 + 77.89)\lambda^2 \\ &+ (1155V_0^2 - 232)\lambda + 150 = 0. \end{aligned} \tag{3.7}$$

The system's critical instability velocity $V_c = 0.45$ can be obtained by solving the formula $66V_0^2 - 13.1 = 0$ using the Routh criterion. When the coke driving velocity is higher than this value, the pushing device operates stably. When the coke driving velocity is lower than this value, the pushing device operates unstably and is more prone to self-excited vibration.

In the purpose of verifying the correctness of the theoretical calculation results, the established friction self-excited vibration system is numerically simulated at different driving velocities. The velocity values are 0.425, 0.435, 0.45, and 0.465, respectively. The simulated phase diagrams and the corresponding displacement curves are shown in Figs. 3 and 4.

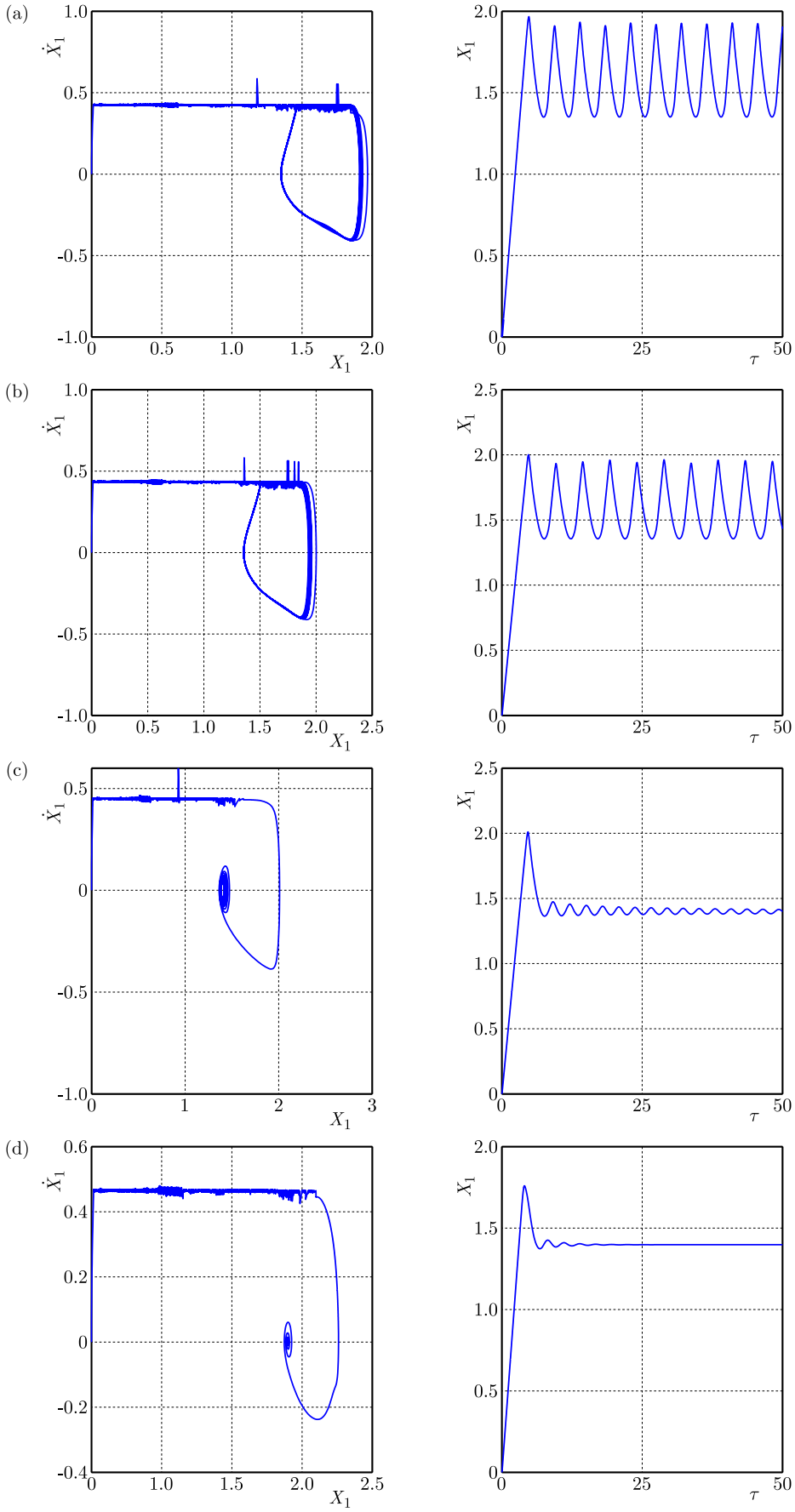

Fig. 3. Simulation phase diagrams and displacement curve diagrams of mass 1 under different driving velocities: (a) $V_0 = 0.425$; (b) $V_0 = 0.435$; (c) $V_0 = 0.45$; (d) $V_0 = 0.465$.

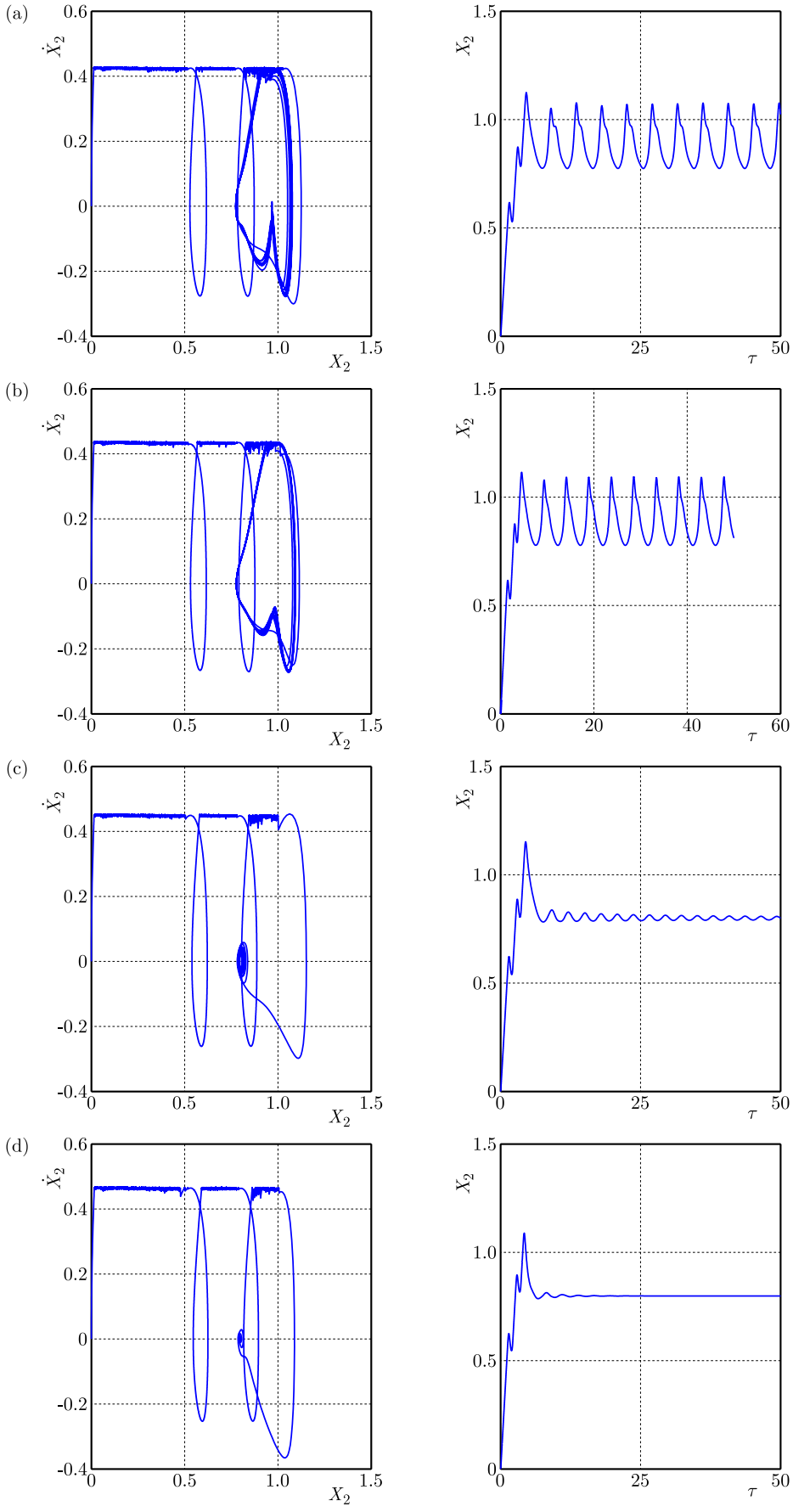

Fig. 4. Simulation phase diagrams and displacement curve diagrams of mass 2 under different driving velocities: (a) $V_0 = 0.425$; (b) $V_0 = 0.435$; (c) $V_0 = 0.45$; (d) $V_0 = 0.465$.

We can see from Fig. 3 and Fig. 4 that when the operating velocity of the device is lower than 0.45, the amplitude of the limit cycle is relatively large, and the equilibrium point of the coke pushing system is in an unstable state. When the operating velocity of the device exceeds 0.45, the amplitude of the limit cycle decreases rapidly, and the equilibrium point of the coke pushing system is in a stable state. It can be seen that in the process of increasing the velocity of the system, the equilibrium point changes from unstable to stable. From the stability analysis of the system, it can be seen that when the driving velocity is 0.45, the Hopf bifurcation phenomenon begins to appear in the system. In order to intuitively show the Hopf bifurcation type of the coke pushing system, the system's bifurcation diagram with the change of the driving velocity is obtained by numerical calculations.

Of course, there are also factors such as friction, damping, or system inertia that can have an impact on bifurcation points and stability. When considering bifurcation cases, such as the transition of a system from rest to motion. The bifurcation point appears when the static friction force is just overcome, and the bifurcation point will change accordingly when the friction factor changes. In the process of motion, friction acts as damping. If the friction factor is large, the stability of the system will be enhanced. As the damping increases, the dynamic behavior of the system changes. The bifurcation point occurs at the transition from undamped periodic motion to damped decayed motion. When the damping exceeds a certain critical value, the properties of the equilibrium point of the system will change and bifurcation will occur. In the case of a two-mass-spring-damping system, the natural frequency of the system changes when one of the masses is changed. The bifurcation point is related to the natural frequency of the system, and the change of mass will lead to the change of the modal characteristics of the system. The amount of inertia (mass) affects how quickly the system responds to external forces. The greater inertia makes the system more difficult to accelerate or slow down. From a stability point of view, systems with high inertia may be less likely to quickly deviate from their equilibrium state when subjected to external disturbances. In general, changes in the parameters of friction, damping and inertia of the system have complex effects on the bifurcation point and stability. They interact with each other, and in different physical systems, the specific manifestation and degree of these effects will vary depending on the specific structure and dynamics of the system. In engineering and physics research, the effects of these parameters on system performance need to be carefully analyzed in order to optimize the system design and control.

The coke pushing device studied in this paper is a practical device, which has been installed and calculated in advance. In actual use, according to the different production stages of the coke pushing device starting from the empty stroke to the coke pushing operation process, the most significant change in system parameters is the operating velocity of the coke pushing device. According to the field observation, it is found that when the coke pushing device starts to push coke, the running velocity of the device will decrease rapidly, resulting in a strong vibration phenomenon, so this paper chooses the sensitive parameter of coke pushing velocity as the bifurcation parameter according to the actual working condition. The controller design is also mainly to solve the vibration control problem caused by the velocity change.

The system's simulation parameters are set as follows: $\mu_s = 0.8$, $\mu_m = 0.6$, $\upsilon_m = 0.45$, $\xi_1 = \xi_2 = 0.1$, $a_1 = a_2 = 0.01$, $\beta = 1$, $\beta_1 = 1.5$, $\beta_2 = \beta_3 = 0.01$. The bifurcation diagrams of the system with respect to the driving velocity are shown in Fig. 5.

It can be found from the bifurcation diagrams that when the velocity is less than 0.45, the system's equilibrium point is in an unstable state, and the motion form is quasi-periodic motion. When the velocity is greater than 0.45, the system's equilibrium point is in a stable state, and each bifurcation diagram appears as a single-valued curve. This indicates that the equilibrium point of the coke pushing system will gradually transit from an unstable to a stable state as the system's velocity increases. When the driving velocity increases to 0.45, the system begins to exhibit the supercritical Hopf bifurcation. Therefore, in the purpose of improving the stability of the coke pushing device and reduce the intensity of the friction self-excited vibration of the

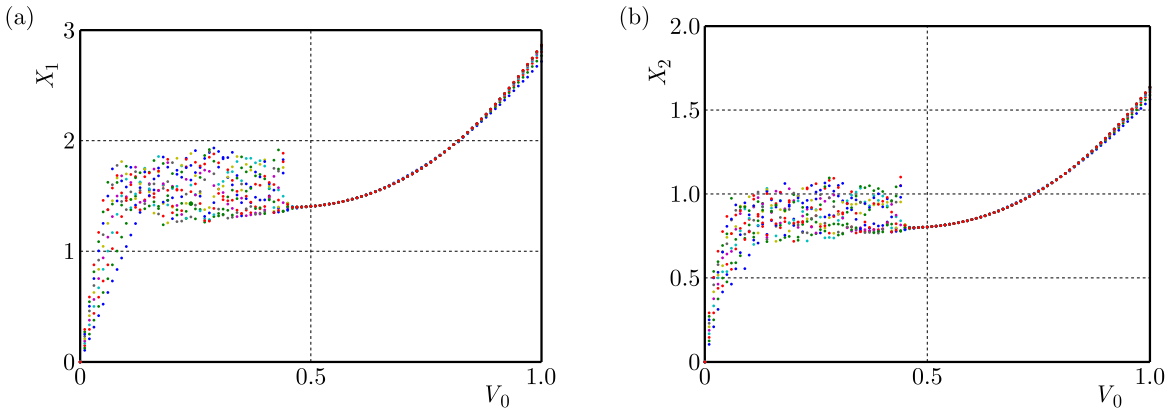

Fig. 5. System's bifurcation diagrams along with the driving velocity: (a) bifurcation diagram of mass 1 with respect to the driving velocity; (b) bifurcation diagram of mass 2 with respect to the driving velocity.

device, a linear and nonlinear state feedback controller is introduced at the critical bifurcation velocity of 0.45 to control the coke pushing system.

4. Research on the bifurcation control of coke pushing system

4.1. Research on linear state feedback control

Let $\mu_s = 0.8$, $\mu_m = 0.6$, $\upsilon_m = 0.45$, $\xi_1 = \xi_2 = 0.1$, $a_1 = a_2 = 0.01$, $\beta = 1$, $\beta_1 = 1.5$, $\beta_2 = \beta_3 = 0.01$. Applying the linear feedback control to the coke pushing system (Eq. (2.6)), it can be obtained that:

$$\begin{aligned} \dot{Y}_1 &= Y_2, \qquad \dot{Y}_2 = -0.1(Y_2 - Y_4) - 10Y_1 + 10Y_3 + 10\mu_1 + k_1 Y_2, \\ \dot{Y}_3 &= Y_4, \qquad \dot{Y}_4 = -0.2Y_4 + 0.1Y_2 + 10Y_1 - 25Y_3 + 10\mu_2. \end{aligned} \tag{4.1}$$

Here, $\mu_1 = 0.8 + 0.67(Y_2 - V_0) - 1.1(Y_2 - V_0)^3$, $\mu_2 = 0.8 + 0.67(Y_4 - V_0) - 1.1(Y_4 - V_0)^3$, k_1 is the linear gain of the designed controller, $k_1 \neq 0$, the introduction of the linear part of the controller does not change the equilibrium point of the original system. When the friction force takes only the linear part, the expressions of friction coefficients are, respectively, simplified as: $\mu_1 = 0.67(Y_2 - V_0) - 3.3V_0^2 Y_2$, $\mu_2 = 0.67(Y_4 - V_0) - 3.3V_0^2 Y_4$. When V_0 is 0.45, the Jacobian matrix of the linear part of system (Eq. (4.1)) at the equilibrium point is

$$\mathbf{A} = \begin{bmatrix} 0 & 1 & 0 & 0 \\ -10 & k_1 - 0.0825 & 10 & 0.1 \\ 0 & 0 & 0 & 1 \\ 10 & 0.1 & -25 & -0.1825 \end{bmatrix}. \tag{4.2}$$

The characteristic equation of matrix $\mathbf{A}$ is

$$\lambda^4 + (0.265 - k_1)\lambda^3 + (35.005 - 0.1825k_1)\lambda^2 + (1.8875 - 25k_1)\lambda + 150 = 0. \tag{4.3}$$

In order to satisfy the Routh–Hurwitz stability criterion and ensure that the roots of the characteristic Eq. (4.3) all have negative real parts, then

$$\begin{aligned} &0.265 - k_1 > 0, \qquad 35.005 - 0.1825k_1 > 0, \qquad 1.8875 - 25k_1 > 0, \\ &(0.265 - k_1)(35.005 - 0.1825k_1) - (1.8875 - 25k_1) > 0, \\ &(0.265 - k_1)(35.005 - 0.1825k_1)(1.8875 - 25k_1) - (1.8875 - 25k_1)^2 - 150(0.265 - k_1)^2 > 0, \end{aligned} \tag{4.4}$$

that is

$$\begin{aligned} &k_1 < 0.265, \qquad k_1 < 191.808, \qquad k_1 < 0.0755, \\ &k_1 < 0.745 \qquad \text{or} \qquad k_1 > 54.342, \\ &k_1 < 0.028 \qquad \text{or} \qquad 1.267 < k_1 < 20.99. \end{aligned} \tag{4.5}$$

In summary, $k_1 \in (-\infty, 0) \cup (0, 0.028)$.

To verify the correctness of the theoretical calculation, V_0 is set to 0.45 and the other parameters remain unchanged. The k_1 is set to -0.1, -0.5, -0.8, respectively, and the system (Eq. (4.1)) is simulated and analyzed. The phase diagrams and time-domain displacement waveform diagrams are shown in Figs. 6 and 7.

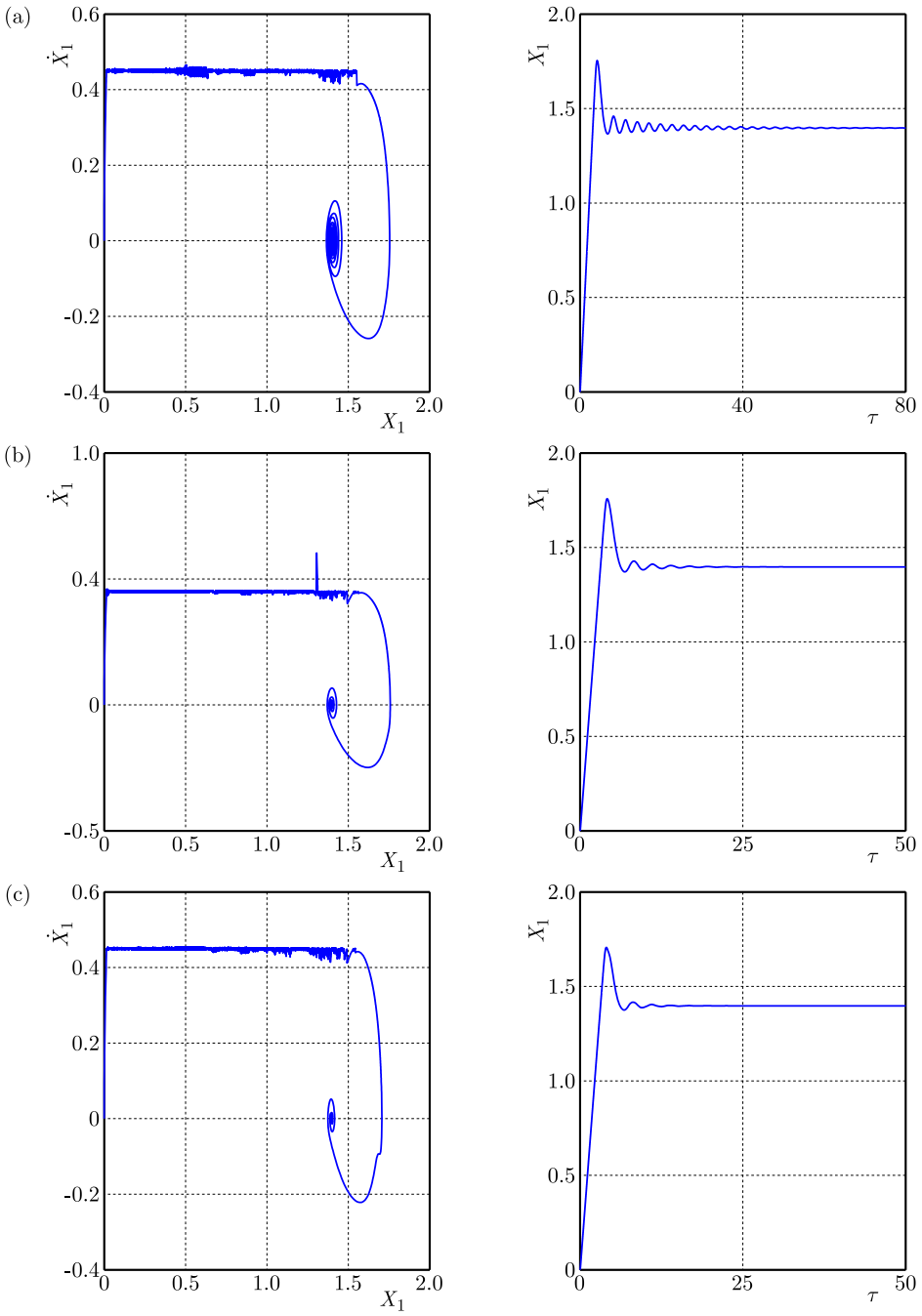

Fig. 6. Phase diagrams and the corresponding displacement curves of mass 1 when the linear gain k_1 takes different values: (a) $k_1 = -0.1$; (b) $k_1 = -0.5$; (c) $k_1 = -0.8$.

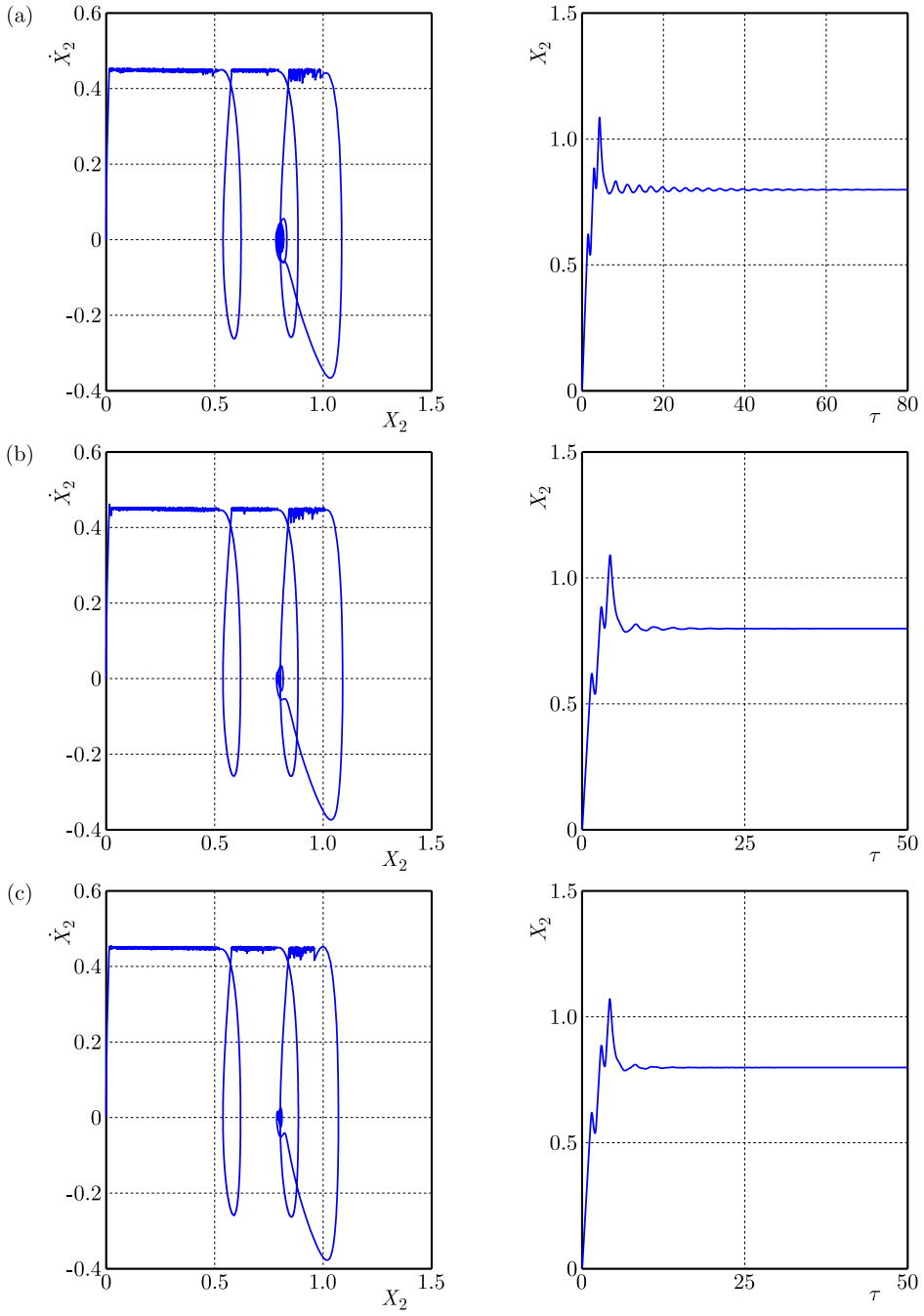

Fig. 7. Phase diagrams and the corresponding displacement curves of the mass 2 when the linear gain k_1 takes different values: (a) $k_1 = -0.1$; (b) $k_1 = -0.5$; (c) $k_1 = -0.8$.

From the simulation results of Fig. 6 and Fig. 7, it can be clearly seen that when the linear gain k_1 takes -0.1, -0.5, -0.8, compared with the phase diagrams and displacement curve diagrams without control (Figs. 3c and 4c), the limit cycle disappears and the system stabilizes to the equilibrium point after the control is applied. It can be seen that when the appropriate parameter k_1 is selected, the Hopf bifurcation phenomenon can be eliminated near the original bifurcation point, the Hopf bifurcation point is changed, the supercritical Hopf bifurcation occurs in advance, and the motion stability of pushing coke is improved. Meanwhile, the simulation results from Fig. 3 to Fig. 7 show that the bifurcation points of the critical velocity of mass 1 and mass 2 are the same, and the change trends of the motion affected by the velocity are the same, and the motions are also carried out according to the similar trend after being controlled,

which indicates that after controlling mass 1, mass 2 can be affected synchronously with mass 1. Limited in space, we only study the influence of the controller on mass 1.

For the purpose of studying the influence of different values of k_1 on the Hopf bifurcation point, the values of other parameters remain unchanged, V_0 is set to 0.44 and 0.43, k_1 is set to -0.1, -0.8, -1.4, respectively, and the system (Eq. (4.1)) is simulated and analyzed. The phase diagrams and time-domain displacement waveform diagrams are shown in Figs. 8 and 9, respectively.

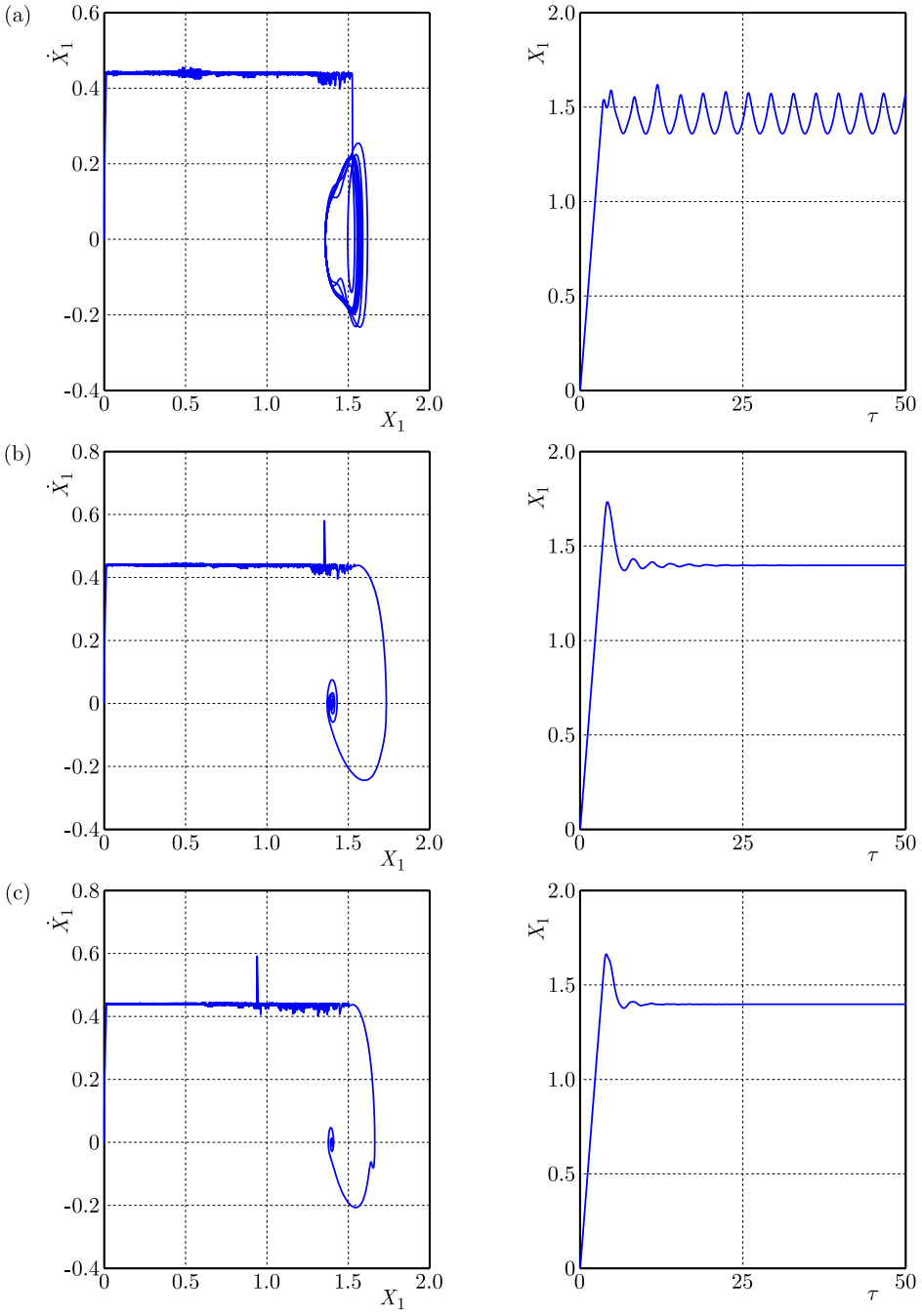

Fig. 8. Phase diagrams and corresponding displacement curves of mass 1 when V_0 is 0.44 and linear gain k_1 is different: (a) $k_1 = -0.1$; (b) $k_1 = -0.8$; (c) $k_1 = -1.4$.

Through the analysis of the simulation results in Fig. 8a, we can intuitively find that when V_0 is 0.44 and k_1 is -0.1, the Hopf bifurcation behavior of the system is not eliminated. Compared with Fig. 6a, it can be seen that when k_1 is -0.1, the bifurcation velocity of the coke pushing

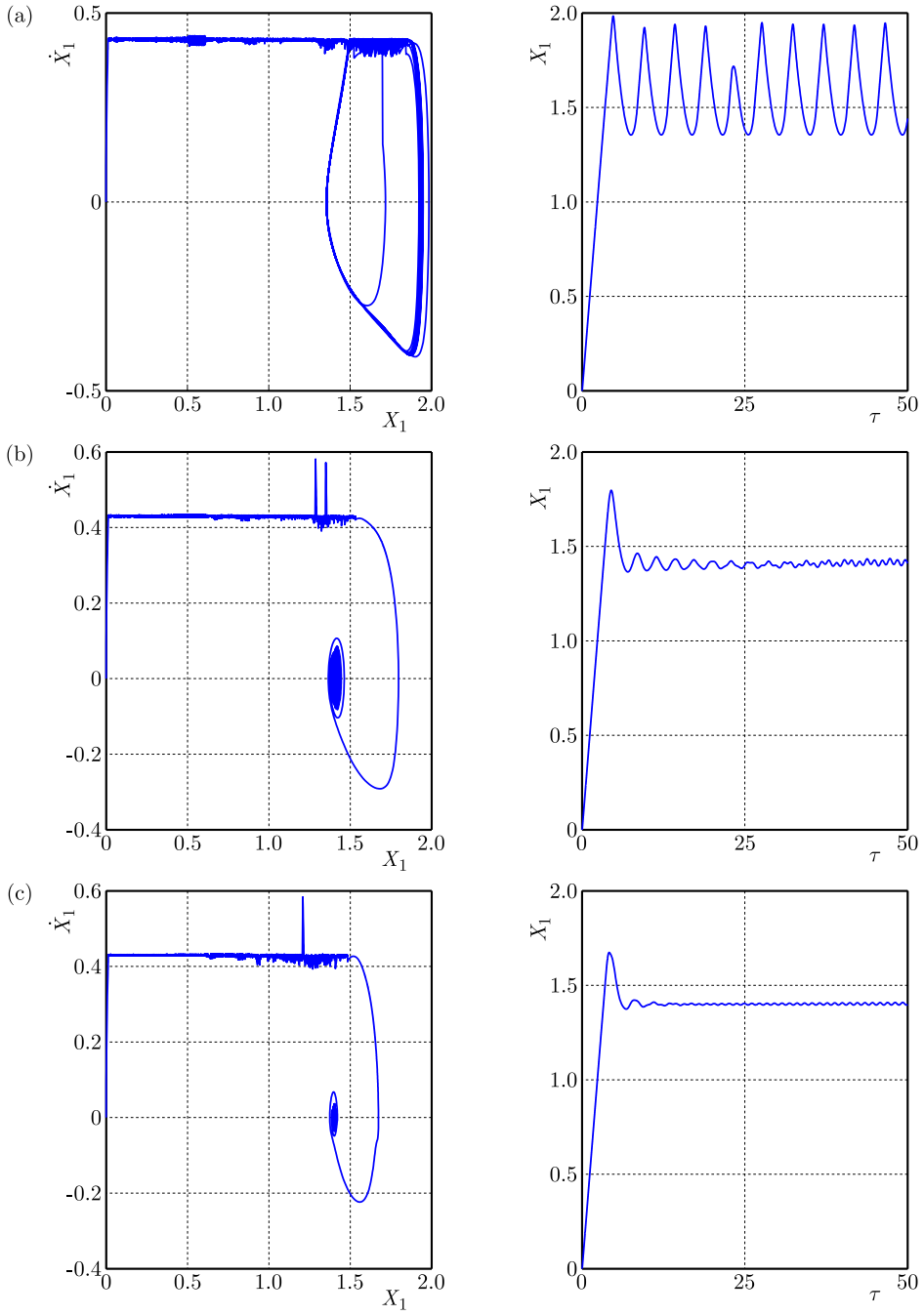

Fig. 9. Phase diagrams and corresponding displacement curves of mass 1 when V_0 is 0.43 and linear gain k_1 is different: (a) $k_1 = -0.1$; (b) $k_1 = -0.8$; (c) $k_1 = -1.4$.

system can be advanced from 0.45 to 0.44. As the value of k_1 continues to decrease, the system gradually stabilizes to the equilibrium point, and the Hopf bifurcation behavior of the system disappears. Comparing Fig. 8b and 8c with Fig. 9b and 9c, we can find that when k_1 is -0.8, -1.4, the bifurcation velocity of the coke pushing system can be advanced from 0.45 to 0.43. The simulation analysis results in Fig. 9 show that with the decrease of k_1, the control effect on the coke pushing system is more and more significant, but the bifurcation behavior of the system is not eliminated. This shows that to a certain extent, selecting a smaller k_1 value is conducive to reducing the critical bifurcation velocity of the coke pushing system, and then to achieve the stable operation of the coke pushing device at a lower operating velocity and reduce the possibility of self-excited vibration.

4.2. Research on nonlinear state feedback control

The linear part of the controller can control the change of the bifurcation point of the system, thus, the motion state of the system can be well improved. However, the linear part of the controller has no effective control effect on the limit cycle. Cui *et al.* (2012) show that the design of a suitable nonlinear state controller can effectively reduce the amplitude of the limit cycle, so as to control the amplitude of the periodic solution generated by the bifurcation. In view of this, this section studies the influence of nonlinear state feedback control on the vibration amplitude of the self-excited vibration system.

Let $\mu_s = 0.8$, $\mu_m = 0.6$, $\upsilon_m = 0.45$, $\xi_1 = \xi_2 = 0.1$, $a_1 = a_2 = 0.01$, $\beta = 1$, $\beta_1 = 1.5$, $\beta_2 = \beta_3 = 0.01$. By applying nonlinear feedback control to the coke pushing system (Eq. (2.6)), we can obtain:

$$\begin{aligned} \dot{Y}_1 &= Y_2, \qquad \dot{Y}_2 = -0.1(Y_2 - Y_4) - 10Y_1 + 10Y_3 + 10\mu_1 + k_2 Y_2^3, \\ \dot{Y}_3 &= Y_4, \qquad \dot{Y}_4 = -0.2Y_4 + 0.1Y_2 + 10Y_1 - 25Y_3 + 10\mu_2. \end{aligned} \tag{4.6}$$

Here, $\mu_1 = 0.8 + 0.67(Y_2 - V_0) - 1.1(Y_2 - V_0)^3$, $\mu_2 = 0.8 + 0.67(Y_4 - V_0) - 1.1(Y_4 - V_0)^3$, k_2 is the nonlinear gain of the designed controller, $k_2 \neq 0$, and the introduction of the nonlinear part of the controller does not change the equilibrium point of the original system. When the friction force is only a linear part, the friction coefficient expressions are simplified as: $\mu_1 = 0.67(Y_2 - V_0) - 3.3V_0^2 Y_2$, $\mu_2 = 0.67(Y_4 - V_0) - 3.3V_0^2 Y_4$. Then system (Eq. (4.6)) can be written as follows:

$$\dot{\mathbf{Y}} = \mathbf{B}\mathbf{Y} + \mathbf{C}\mathbf{Q}. \tag{4.7}$$

When V_0 is 0.45, the expressions of matrices $\mathbf{B}$, $\mathbf{Y}$, $\mathbf{C}$, and $\mathbf{Q}$ are

$$\mathbf{B} = \begin{bmatrix} 0 & 1 & 0 & 0 \\ -10 & -0.0825 & 10 & 0.1 \\ 0 & 0 & 0 & 1 \\ 10 & 0.1 & -25 & -0.1825 \end{bmatrix}, \tag{4.8}$$

$$\mathbf{Y} = [\, Y_1 \;\; Y_2 \;\; Y_3 \;\; Y_4 \,]^{\mathrm{T}}, \tag{4.9}$$

$$\mathbf{C} = [\, 0 \;\; 1 \;\; 0 \;\; 0 \,]^{\mathrm{T}}, \tag{4.10}$$

$$\mathbf{Q} = [k_2 Y_2^3]. \tag{4.11}$$

The characteristic equation corresponding to the matrix $\mathbf{B}$ is

$$\lambda^4 + 0.265\lambda^3 + 35.0051\lambda^2 + 1.8875\lambda + 150 = 0. \tag{4.12}$$

According to Eq. (4.12), the characteristic roots of the system are $\lambda_1 = -0.0112 + 2.2361i$, $\lambda_2 = -0.0112 - 2.2361i$, $\lambda_3 = -0.1213 + 5.4758i$, $\lambda_4 = -0.1213 - 5.4758i$. The eigenvector matrix corresponding to the characteristic roots is

$$\begin{aligned} \mathbf{D} &= [\, v_1 \;\; v_2 \;\; v_3 \;\; v_4 \,] \\ &= \begin{bmatrix} -0.0018 - 0.3651i & -0.0018 + 0.3651i & 0.0009 + 0.0803i & 0.0009 - 0.0803i \\ 0.8165 & 0.8165 & -0.4400 - 0.0048i & -0.4400 + 0.0048i \\ -0.0001 - 0.1826i & -0.0001 + 0.1826i & -0.0036 - 0.1606i & -0.0036 + 0.1606i \\ 0.4083 + 0.0018i & 0.4083 - 0.0018i & 0.8798 & 0.8798 \end{bmatrix}. \end{aligned} \tag{4.13}$$

Let $\mathbf{Y} = \mathbf{TU}$, where the matrices $\mathbf{T}$ and $\mathbf{U}$ are

$$\mathbf{T} = [\operatorname{Re} v_3, -\operatorname{Im} v_3, \operatorname{Re} v_1, -\operatorname{Im} v_1] = \begin{bmatrix} 0.0009 & -0.0803 & -0.0018 & 0.3651 \\ -0.44 & 0.0048 & 0.8165 & 0 \\ -0.0036 & 0.1606 & -0.0001 & 0.1826 \\ 0.8798 & 0 & 0.4083 & -0.0018 \end{bmatrix}, \tag{4.14}$$

$$\mathbf{U} = [\, U_1 \;\; U_2 \;\; U_3 \;\; U_4 \,]^{\mathrm{T}}. \tag{4.15}$$

Then the system (Eq. (4.7)) can be reduced to the following form:

$$\begin{aligned} \dot{U}_1 &= -0.1201U_1 - 5.4756U_2 + G_1(U_1, U_2, U_3, U_4, k_2), \\ \dot{U}_2 &= 5.4760U_1 - 0.1224U_2 + G_2(U_1, U_2, U_3, U_4, k_2), \\ \dot{U}_3 &= -0.0115U_3 - 2.2359U_4 + G_3(U_1, U_2, U_3, U_4, k_2), \\ \dot{U}_4 &= 2.2363U_3 - 0.0110U_4 + G_4(U_1, U_2, U_3, U_4, k_2), \end{aligned} \tag{4.16}$$

where G_1, G_2, G_3, G_4 are expressed as

$$\begin{aligned} G_1(U_1, U_2, U_3, U_4, k_2) &= -0.4547k_2(-0.44U_1 + 0.0048U_2 + 0.8165U_3)^3, \\ G_2(U_1, U_2, U_3, U_4, k_2) &= -0.0131k_2(-0.44U_1 + 0.0048U_2 + 0.8165U_3)^3, \\ G_3(U_1, U_2, U_3, U_4, k_2) &= 0.9798k_2(-0.44U_1 + 0.0048U_2 + 0.8165U_3)^3, \\ G_4(U_1, U_2, U_3, U_4, k_2) &= 0.0031k_2(-0.44U_1 + 0.0048U_2 + 0.8165U_3)^3. \end{aligned} \tag{4.17}$$

The stability index σ_2 of the Hopf bifurcation in Eq. (4.18) can be calculated by substituting Eq. (4.17) into Appendix or the formulas in (Liu & Tang, 2008) and (Hassard, 1981):

$$\begin{aligned} \sigma_2 &= 2\operatorname{Re}\left\{ \frac{g_{20}g_{11} - 2\left|g_{11}\right|^2 - \frac{1}{3}\left|g_{02}\right|^2}{2\omega_0} i + \frac{g_{21}}{2} \right\} \\ &= \operatorname{Re}\left\{k_2(0.0012i + 0.029)\right\} = 0.029k_2. \end{aligned} \tag{4.18}$$

When $k_2 < 0$, $\sigma_2 < 0$, the Hopf bifurcation stability of the coke pushing system can be guaranteed. Next, the numerical calculation method is used to study the influence of the change of the nonlinear gain k_2 on the size of the limit cycle. The purpose is to determine a reasonable parameter range to improve the working condition of the coke pushing system, so as to reduce the self-excited vibration phenomenon of the pushing coke process.

For research on the influence of k_2 on the motion state of the coke pushing device at different velocities, the V_0 is set as 0.44, 0.43, 0.42, and the k_2 is set as -1, -10, and -20, respectively, for simulation analysis. The phase diagrams and displacement curves of the system are shown in Figs. 10–12.

From Figs. 10–12, it can be seen that the nonlinear gain k_2 can effectively control the limit cycle amplitude of the system. From the phase diagrams, it is found that with the continuous decrease of the nonlinear gain k_2, the overall trend of the limit cycle amplitude of the coke pushing system is gradually reduced. From the displacement curves, it is found that the displacement fluctuation amplitude is also gradually reduced, indicating that the control effect is more obvious during the decrease of the nonlinear gain k_2. Comparing with Fig. 10, Fig. 11, and Fig. 12, we can also see that when the nonlinear gain k_2 takes the same value, the closer the driving velocity is to the bifurcation velocity 0.45, the more significant the nonlinear gain control effect is.

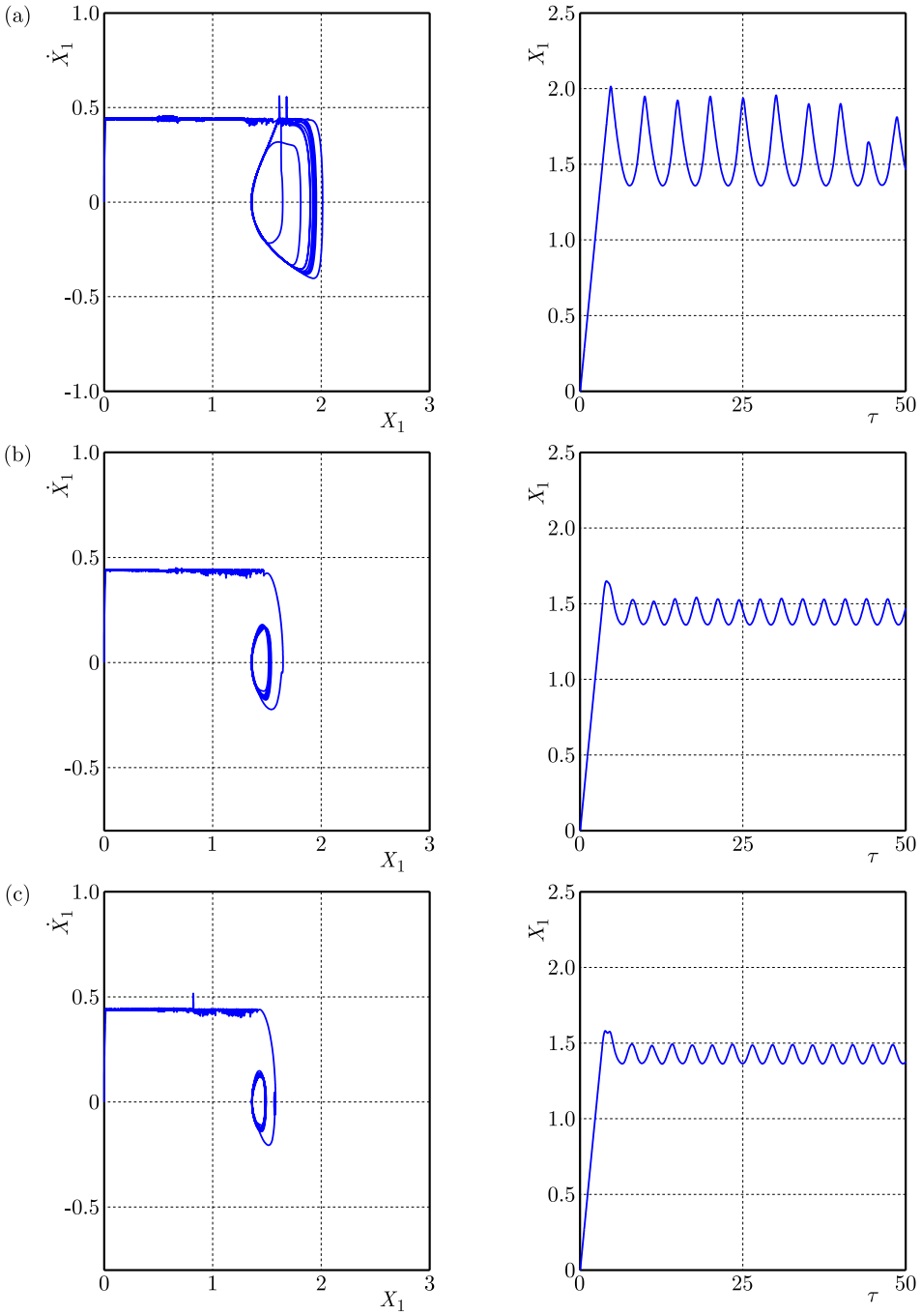

Fig. 10. Phase diagrams and the corresponding displacement curves when V_0 is 0.44 and nonlinear gain k_2 is set as different values: (a) $k_2 = -1$; (b) $k_2 = -10$; (c) $k_2 = -20$.

Therefore, the reasonable selection of nonlinear gain can effectively reduce the amplitude of the limit cycle, and then reduce the self-excited vibration of the pushing coke process.

To characterize the effect of simultaneous control of linear and nonlinear parts of the controller proposed in this article, the linear gain k_1 is taken as -0.8, and the nonlinear gain k_2 is taken as -10. Then the motion behaviour of the coke pushing device under different running velocities is controlled. For an intuitive comparison with Figs. 3a to 3c, the driving velocity V_0 of the system is set to 0.425, 0.435, and 0.45, respectively, on the basis of other parameters unchanged. The coke pushing system is numerically simulated, and the obtained phase diagrams and the corresponding displacement curves are shown in Fig. 13.

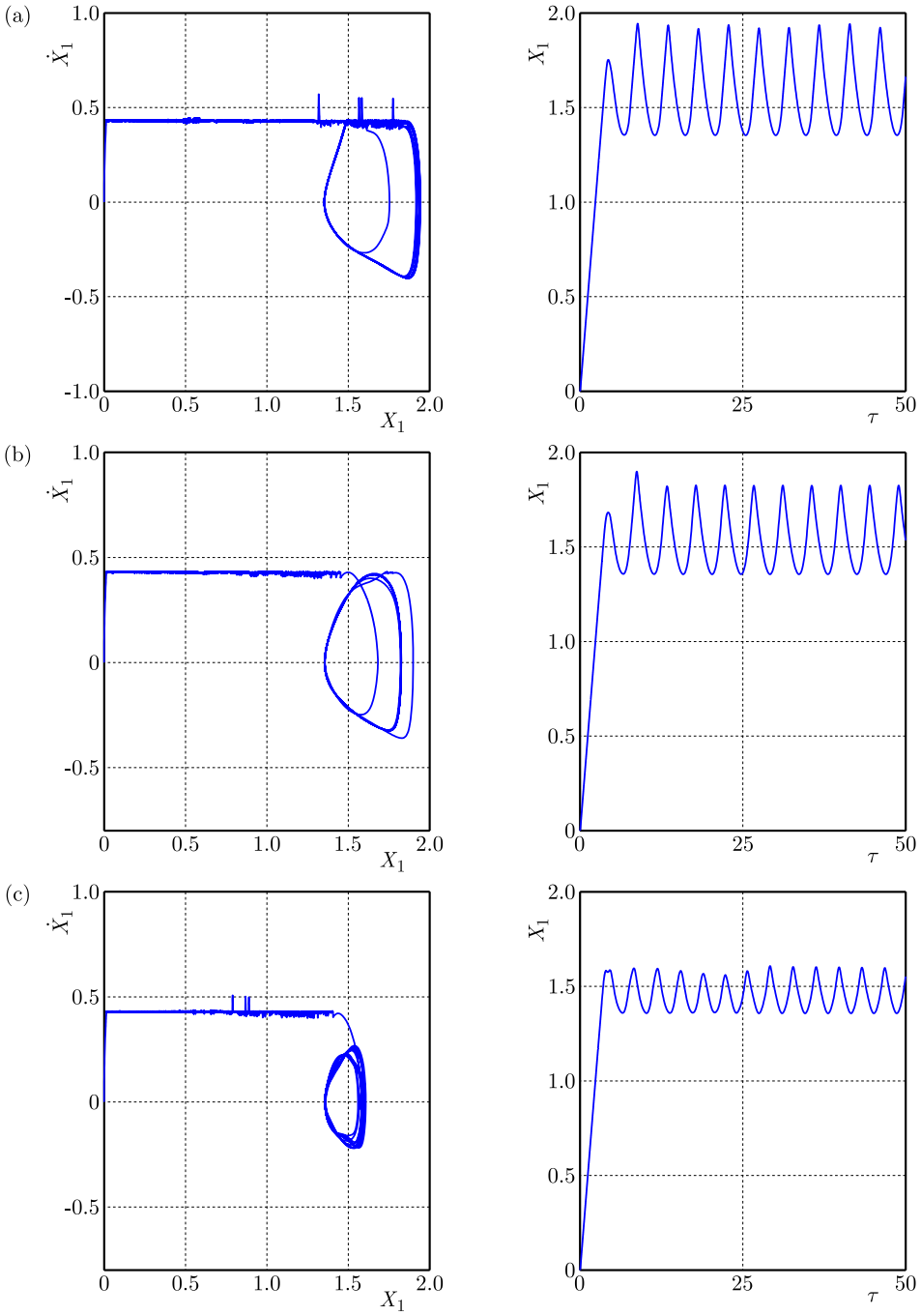

Fig. 11. Phase diagrams and the corresponding displacement curves when V_0 is 0.43 and nonlinear gain k_2 is set as different values: (a) $k_2 = -1$; (b) $k_2 = -10$; (c) $k_2 = -20$.

From the phase diagrams and displacement curve diagrams of Fig. 13, we can see that the motion state of the coke pushing system is obviously improved after the controller is applied. By comparing Fig. 13a and Fig. 3a, it can be clearly observed that the vibration amplitude of the system is significantly reduced after the controller designed in this paper is applied. The comparison result of Fig. 13b and Fig. 3b indicates that the vibration amplitude of the coke pushing system is greatly reduced after applying the controller designed in this paper, but the bifurcation phenomenon of the system is not eliminated. By comparing Fig. 13c and Fig. 3c, it is found that the limit cycle disappears and the coke pushing system stabilizes to the equilibrium point after applying the controller designed in this paper. On the whole, the control effect on the

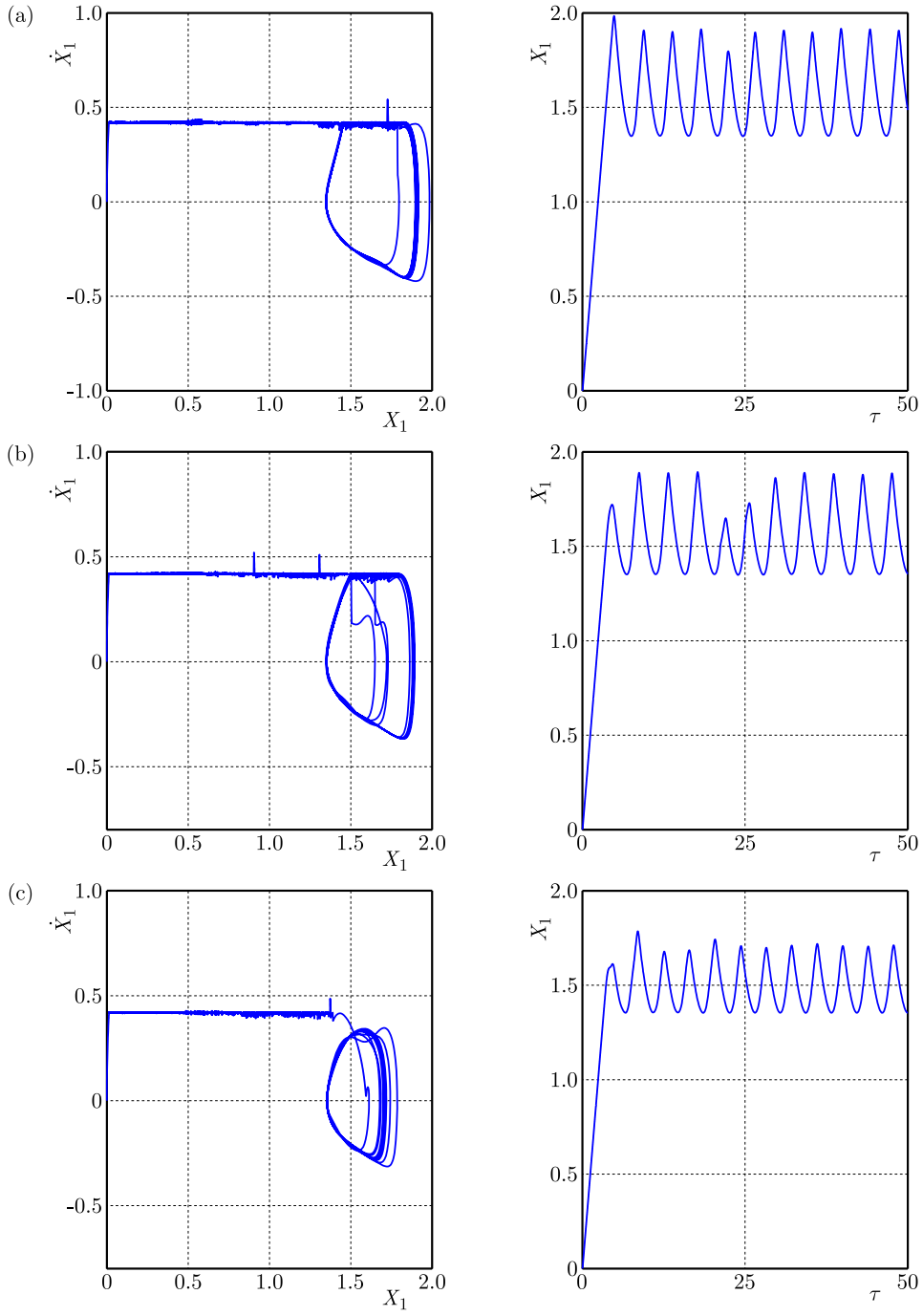

Fig. 12. Phase diagrams and the corresponding displacement curves when V_0 is 0.42 and nonlinear gain k_2 is set as different values: (a) $k_2 = -1$; (b) $k_2 = -10$; (c) $k_2 = -20$.

coke pushing system is more obvious when the driving velocity is closer to the critical bifurcation point, which is consistent with the previous results when linear gain and nonlinear gain acting alone.

5. Conclusions

According to the fact that part of the coke rod is located in the carbonization room and part is located outside the carbonization room, the frictional self-excited vibration model of the double -mass-conveyor belt is established to study the friction-induced vibration characteristics

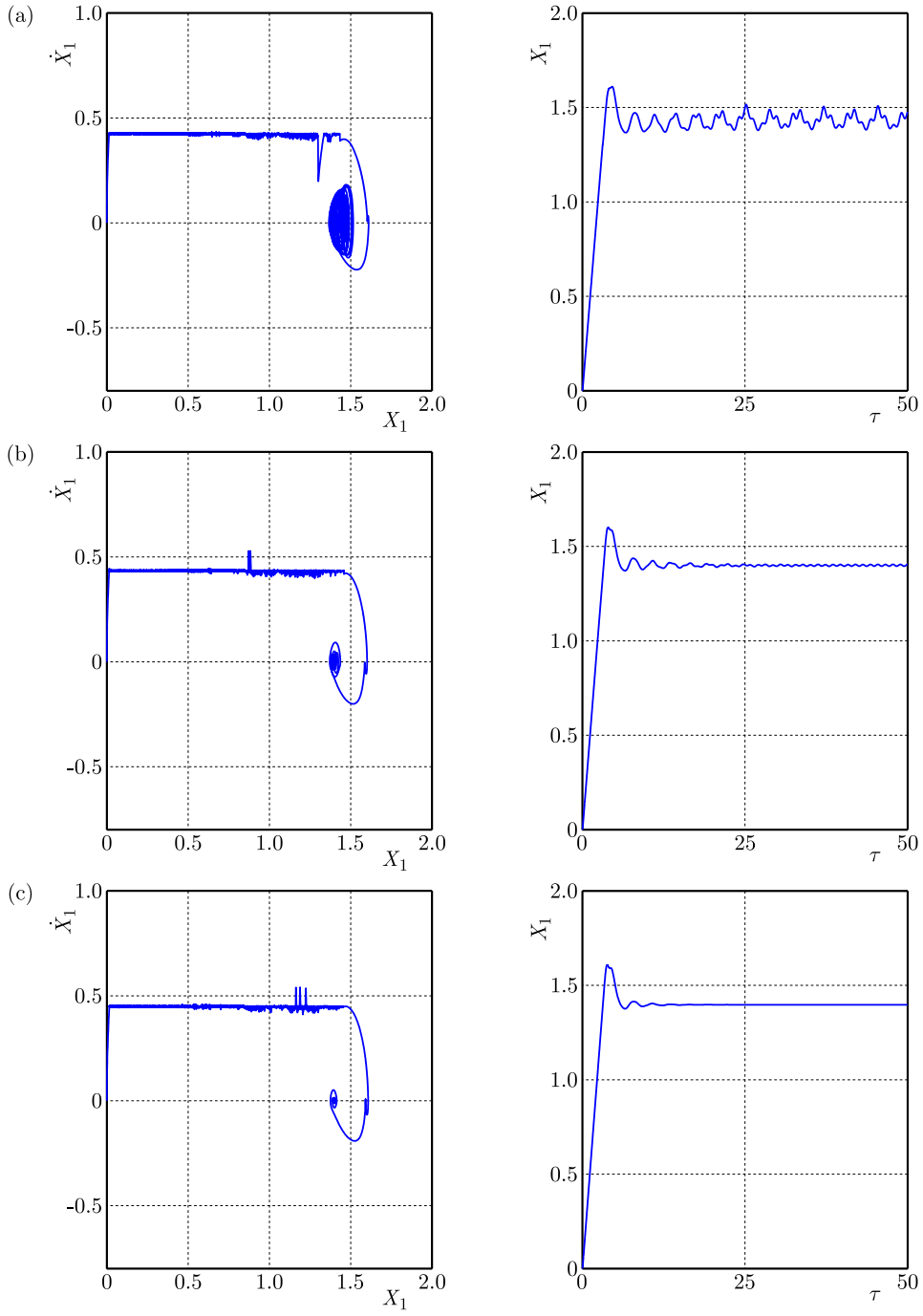

Fig. 13. Comprehensive control effect of the controller designed in this paper when V_0 takes different values: (a) $V_0 = 0.425$; (b) $V_0 = 0.435$; (c) $V_0 = 0.45$.

of pushing coke progress. The critical instability velocity of the coke pushing system is obtained by theoretical calculations and verified by numerical simulation. Then, the bifurcation characteristics of the system are analyzed, and the linear and nonlinear state feedback controllers are proposed to control the bifurcation behaviours of the system. Numerical simulation shows the effectiveness of the control effect. The specific conclusions are as follows:

– The newly established dynamic model of the system divides the coke pushing system into two bodies, which can better simulate the running state of the coke pushing device, that is, the part that enters the carbonization room and the part that stays outside the carbonization room.

– Both the critical instability velocity and bifurcation velocity of the coke pushing system are 0.45. When the driving velocity exceeds this value, the system is stable to the equilibrium point. When the driving velocity does not reach this value, the coke pushing system is in an unstable state and the self-excited vibration phenomenon is easy to occur. When the drive velocity reaches 0.45, the system begins to appear the supercritical Hopf bifurcation.
– The linear gain of the designed controller has an important effect on the Hopf bifurcation point of the coke pushing system. Choosing a smaller linear gain can reduce the Hopf bifurcation velocity and help the system work stably at a lower velocity. The nonlinear gain of the designed controller has an important effect on the limit cycle of the coke pushing system. The smaller nonlinear gain can reduce the amplitude of the limit cycle of the system, and then alleviate the friction self-excited vibration of the system.

Appendix. Coefficients in Eq. (4.18)

$$g_{20} = \frac{1}{4}\left\{\frac{\partial^2 G_1}{\partial U_1^2} - \frac{\partial^2 G_1}{\partial U_2^2} + 2\frac{\partial^2 G_2}{\partial U_1 \partial U_2} + i\left[\frac{\partial^2 G_2}{\partial U_1^2} - \frac{\partial^2 G_2}{\partial U_2^2} - 2\frac{\partial^2 G_1}{\partial U_1 \partial U_2}\right]\right\},$$

$$g_{11} = \frac{1}{4}\left\{\frac{\partial^2 G_1}{\partial U_1^2} + \frac{\partial^2 G_1}{\partial U_2^2} + i\left[\frac{\partial^2 G_2}{\partial U_1^2} + \frac{\partial^2 G_2}{\partial U_2^2}\right]\right\},$$

$$g_{02} = \frac{1}{4}\left\{\frac{\partial^2 G_1}{\partial U_1^2} - \frac{\partial^2 G_1}{\partial U_2^2} - 2\frac{\partial^2 G_2}{\partial U_1 \partial U_2} + i\left[\frac{\partial^2 G_2}{\partial U_1^2} - \frac{\partial^2 G_2}{\partial U_2^2} + 2\frac{\partial^2 G_1}{\partial U_1 \partial U_2}\right]\right\},$$

$$g_{21} = G_{21} + 2G_{110}^1\omega_{11}^1 + G_{101}^1\omega_{20}^1 + 2G_{110}^2\omega_{11}^2 + G_{101}^2\omega_{20}^2,$$

where

$$G_{21} = \frac{1}{8}\left\{\frac{\partial^3 G_1}{\partial U_1^3} + \frac{\partial^3 G_1}{\partial U_1 \partial U_2^2} + \frac{\partial^3 G_2}{\partial U_1^2 \partial U_2} + \frac{\partial^3 G_2}{\partial U_2^3} + i\left[\frac{\partial^3 G_2}{\partial U_1^3} + \frac{\partial^3 G_2}{\partial U_1 \partial U_2^2} - \frac{\partial^3 G_1}{\partial U_1^2 \partial U_2} - \frac{\partial^3 G_1}{\partial U_2^3}\right]\right\},$$

$$G_{110}^1 = \frac{1}{2}\left\{\frac{\partial^2 G_1}{\partial U_1 \partial U_3} + \frac{\partial^2 G_2}{\partial U_2 \partial U_3} + i\left[\frac{\partial^2 G_2}{\partial U_1 \partial U_3} - \frac{\partial^2 G_1}{\partial U_2 \partial U_3}\right]\right\},$$

$$G_{110}^2 = \frac{1}{2}\left\{\frac{\partial^2 G_1}{\partial U_1 \partial U_4} + \frac{\partial^2 G_2}{\partial U_2 \partial U_4} + i\left[\frac{\partial^2 G_2}{\partial U_1 \partial U_4} - \frac{\partial^2 G_1}{\partial U_2 \partial U_4}\right]\right\},$$

$$G_{101}^1 = \frac{1}{2}\left\{\frac{\partial^2 G_1}{\partial U_1 \partial U_3} - \frac{\partial^2 G_2}{\partial U_2 \partial U_3} + i\left[\frac{\partial^2 G_2}{\partial U_1 \partial U_3} + \frac{\partial^2 G_1}{\partial U_2 \partial U_3}\right]\right\},$$

$$G_{101}^2 = \frac{1}{2}\left\{\frac{\partial^2 G_1}{\partial U_1 \partial U_4} - \frac{\partial^2 G_2}{\partial U_2 \partial U_4} + i\left[\frac{\partial^2 G_2}{\partial U_1 \partial U_4} + \frac{\partial^2 G_1}{\partial U_2 \partial U_4}\right]\right\},$$

$$\omega_{11}^1 = -\frac{1}{4\lambda_3(V_c)}\left[\frac{\partial^2 G_3}{\partial U_1^2} + \frac{\partial^2 G_3}{\partial U_2^2}\right],$$

$$\omega_{11}^2 = -\frac{1}{4\lambda_4(V_c)}\left[\frac{\partial^2 G_4}{\partial U_1^2} + \frac{\partial^2 G_4}{\partial U_2^2}\right],$$

$$\omega_{20}^1 = \frac{1}{4(2i\omega_0 - \lambda_3(V_c))}\left[\frac{\partial^2 G_3}{\partial U_1^2} - \frac{\partial^2 G_3}{\partial U_2^2} - 2i\frac{\partial^2 G_3}{\partial U_1 \partial U_2}\right],$$

$$\omega_{20}^2 = \frac{1}{4(2i\omega_0 - \lambda_3(V_c))}\left[\frac{\partial^2 G_4}{\partial U_1^2} - \frac{\partial^2 G_4}{\partial U_2^2} - 2i\frac{\partial^2 G_4}{\partial U_1 \partial U_2}\right].$$

The derivatives of the above are all at zero point, and the bifurcation parameter is the bifurcation value.

Acknowledgments

The authors gratefully acknowledge the financial support by the Basic Research Program of Shanxi Province of China (grant no. 20210302124203).

References

1. Brunetti, J., Massi, F., D'Ambrogio, W., & Berthier, Y. (2016). A new instability index for unstable mode selection in squeal prediction by complex eigenvalue analysis. *Journal of Sound and Vibration*, *377*, 106–122. https://doi.org/10.1016/j.jsv.2016.05.002
2. Chen, J., Sun, H., Gao, H., Fan, Y., & Xu, B. (2019). Modeling, stability and stick-slip behaviour analysis of coke pushing system. *Tribology International*, *136*, 105–113. https://doi.org/10.1016/j.triboint.2019.03.057
3. Chen, J., Sun, H., Jiao, T., Liu, Z., & Xu, B. (2020). Stick-slip vibration analysis and vibration frequency extraction of coke pushing system. *Engineering Failure Analysis*, *108*, Article 104325. https://doi.org/10.1016/j.engfailanal.2019.104325
4. Cui, Y., Liu, S., & Ge, X. (2012). Amplitude control of limit cycle from Hopf bifurcation in the Langford system (in Chinese). *Acta Physica Sinica*, *61*(10), 100202. https://doi.org/10.7498/aps.61.100202
5. Denimal, E., Sinou, J.J., & Nacivet, S. (2020). Generalized Modal Amplitude Stability Analysis for the prediction of the nonlinear dynamic response of mechanical systems subjected to friction-induced vibrations. *Nonlinear Dynamics*, *100*(4), 3121–3144. https://doi.org/10.1007/s11071-020-05627-1
6. Elmaian, A., Gautier, F., Pezerat, C., & Duffal, J.M. (2014). How can automotive friction-induced noises be related to physical mechanisms?. *Applied Acoustics*, *76*, 391–401. https://doi.org/10.1016/j.apacoust.2013.09.004
7. Hassard, B.D., Kazarinoff, N.D., & Wan Y.-H. (1981). Theory and applications of Hopf bifurcation. New York, Cambridge University Press.
8. Kinkaid, N.M., O'Reilly, O.M., & Papadopoulos, P. (2003). Automotive disc brake squeal. *Journal of Sound and Vibration*, *267*(1), 105–166. https://doi.org/10.1016/S0022-460X(02)01573-0
9. Kruse, S., Tiedemann, M., Zeumer, B., Reuss, P., Hetzler, H. & Hoffmann, N. (2015). The influence of joints on friction induced vibration in brake squeal. *Journal of Sound & Vibration*, *340*, 239–252. https://doi.org/10.1016/j.jsv.2014.11.016
10. Li, Z., Wang, X., Zhang, Q., Guan, Z., Mo, J.L., & Ouyang, H. (2018). Model reduction for friction-induced vibration of multi-degree-of-freedom systems and experimental validation. *International Journal of Mechanical Sciences*, *145*, 106–119. https://doi.org/10.1016/j.ijmecsci.2018.06.039
11. Lima, R. & Sampaio, R. (2020). Stick-slip oscillations in a multiphysics system. *Nonlinear Dynamics*, *100*(3), 2215–2224. https://doi.org/10.1007/s11071-020-05677-5
12. Liu, N. & Ouyang, H. (2020). Friction-induced vibration considering multiple types of nonlinearities. *Nonlinear Dynamics*, *102*(4), 2057–2075. https://doi.org/10.1007/s11071-020-06055-x
13. Liu, S.H. & Tang, J.S. (2008). Anti-control of Hopf bifurcation at zero equilibrium of 4D Qi system (in Chinese). *Acta Physica Sinica*, *57*(10), 6162–6168. https://doi.org/10.7498/APS.57.6162
14. Papangelo, A., Hoffmann, N., Grolet, A., Stender, M., & Ciavarella, M. (2018). Multiple spatially localized dynamical states in friction-excited oscillator chains. *Journal of Sound and Vibration*, *417*, 56–64. https://doi.org/10.1016/j.jsv.2017.11.056
15. Pilipchuk, V., Olejnik, P., & Awrejcewicz, J. (2015). Transient friction-induced vibrations in a 2-DOF model of brakes. *Journal of Sound and Vibration*, *344*, 297–312. https://doi.org/10.1016/j.jsv.2015.01.028

16. Popp, K., Hinrichs, N., & Oestreich, M. (1995). Dynamical behaviour of a friction oscillator with simultaneous self and external excitation. *Sādhanā*, *20*(2–4), 627–654. https://doi.org/10.1007/BF02823210

17. Saha, A., Wahi, P., & Bhattacharya, B. (2016). Characterization of friction force and nature of bifurcation from experiments on a single-degree-of-freedom system with friction-induced vibrations. *Tribology International*, *98*, 220–228. https://doi.org/10.1016/j.triboint.2016.02.006

18. Sui, X. & Ding, Q. (2018). Instability and stochastic analyses of a pad-on-disc frictional system in moving interactions. *Nonlinear Dynamics*, *93*(3), 1619–1634. https://doi.org/10.1007/s11071-018-4280-4

19. Thomsen, J.J. & Fidlin, A. (2003). Analytical approximations for stick-slip vibration amplitudes. *International Journal of Non-Linear Mechanics*, *38*(3), 389–403. https://doi.org/10.1016/S0020-7462(01)00073-7

20. Veraszto, Z. & Stepan, G. (2017). Nonlinear dynamics of hardware-in-the-loop experiments on stick–slip phenomena. *International Journal of Non-Linear Mechanics*, *94*, 380–391. https://doi.org/10.1016/j.ijnonlinmec.2017.01.006

21. von Wagner, U., Hochlenert, D., & Hagedorn, P. (2007). Minimal models for disk brake squeal. *Journal of Sound and Vibration*, *302*(3), 527–539. https://doi.org/10.1016/j.jsv.2006.11.023

22. Wang, Q., Wang, Z.W., Mo, J.L., & Zhang, L. (2022). Nonlinear behaviors of the disc brake system under the effect of wheel-rail adhesion. *Tribology International*, *165*, Article 107263. https://doi.org/10.1016/j.triboint.2021.107263

23. Wang, X.C., Huang, B., Wang, R.L., Mo, J.L., & Ouyang, H. (2020). Friction-induced stick-slip vibration and its experimental validation. *Mechanical Systems and Signal Processing*, *142*, Article 106705. https://doi.org/10.1016/j.ymssp.2020.106705

24. Wei, D., Song, J., Nan, Y., & Zhu, W. (2019). Analysis of the stick-slip vibration of a new brake pad with double-layer structure in automobile brake system. *Mechanical Systems and Signal Processing*, *118*, 305–316. https://doi.org/10.1016/j.ymssp.2018.08.055

25. Zhang, L., Wu, J., & Meng, D. (2018). Transient analysis of a flexible pin-on-disk system and its application to the research into time-varying squeal. *Journal of Vibration and Acoustics*, *140*(1), Article 011006. https://doi.org/10.1115/1.4037468

Manuscript received September 13, 2024; accepted for publication January 22, 2025; published online April 8, 2025.